To be published in
IEEE Trans. Nucl. Sci.

BNL# 23345

Presented at IEEE Nuclear Science
Symposium, 19-21 October 1977,
Sheraton Palace Hotel, San Francisco

CONF-771023--40

SECOND COORDINATE READOUT IN DRIFT CHAMBERS BY CHARGE DIVISION*

V. Radeka and P. Rehak

Brookhaven National Laboratory
Upton, New York 11973

October 1977

*This research was supported by the U. S. Department of Energy:
Contract No. EY-76-C-02-0016

DISCLAIMER

To be published in
IEEE Trans. Nucl. Sci.

BNL# 23345

Presented at IEEE Nuclear Science
Symposium, 19-21 October 1977,
Sheraton Palace Hotel, San Francisco

SECOND COORDINATE READOUT IN DRIFT CHAMBERS BY CHARGE DIVISION*

V. Radeka and P. Rehak

Brookhaven National Laboratory
Upton, New York 11973

October 1977

*This research was supported by the U. S. Department of Energy:
Contract No. EY-76-C-02-0016

SECOND COORDINATE READOUT IN DRIFT CHAMBERS BY CHARGE DIVISION*

V. Radeka and P. Rehak

Brookhaven National Laboratory
Upton, New York 11973

Abstract

The drift time measurement and the charge division can be performed simultaneously on the same electrode (resistive anode) without affecting the accuracy of either measurement. It is shown that for the shortest measurement time there is an optimum value for the anode wire resistance. The signal requirement for a position uncertainty $\sigma \leq 0.5\%$ of the anode wire length is only 2.7×10^6 electron charges. The drift chamber can be operated in the linear mode and with negligible space charge effects, so that it can also be used for $\Delta E/\Delta X$ measurements. A simple preamplifier optimized for both the time and charge measurements using a monolithic transistor array is described.

Introduction

Drift chambers appear to be the only practical solution for particle momentum determination in colliding beam experiments. The position resolution required in the azimuthal direction of $\sigma \approx 0.1$ to 0.3 mm rms is difficult to achieve by any other means. The anode wires in such experiments are oriented parallel to the beam axis and to the magnetic field. The problem arises in determining the second coordinate, along this axis, that is along the anode wire. The electron drift enables high position resolution and is therefore used for transverse momentum determination from the curvature of the track in the magnetic field. The second coordinate is used to determine the angle of the particle track to the beam axis and to establish consistency of the particle track, in a multilayer set of concentric chambers, that is, to aid in separating multiple particles. Thus a much higher position uncertainty is sufficient, for example of $\sigma \approx 5$ mm. Nevertheless, the methods used so far have not proven to be satisfactory. An additional proportional chamber with cathode strips in azimuthal direction presents the well known ambiguity problem for multiple particles as well as construction difficulties. A considerable effort has been put into the development of delay lines placed parallel to the anode wire.[1,2,3] This is an obvious approach because of the accuracy and simplicity of delay line readouts. However, delay lines present two problems in this case. One is that they "see" only a fraction of the induced charge since they cover only a fraction of the angle around the anode wire in any practical arrangement considered so far. This requires a large anode signal (if the dead time introduced by the delay line is to be small), which causes significant space charge effects at high event rates and makes the chamber operating conditions critical. The delay line structure is undesirable in the path of the particle because of multiple scattering, and it makes the chamber's construction complex.

Position determination along the anode wire by charge division utilizes the anode signal, and, by allowing the simplest chamber construction, requires no additional material in the path of the particle. In the simplest arrangement the ends of the anode wire are connected directly to the input of low impedance preamplifiers, Fig. 1. The signals are processed separately for charge division and for timing. The pulse shaping for charge division is determined mainly by the charge collection and event rate requirements. Pulse shaping for timing is determined so as to extract with minimum noise the information about the arrival time of the first electrons reaching the vicinity of the anode wire. If the position readout parameters are optimized, the anode signal charge required for good position resolution allows operation of the chambers in the linear mode, so that the energy loss information can also be obtained for particle identification.

In this paper design considerations for this readout are presented with experimental results. Questions important in a large system with many wires are also considered.

Position Readout Design Considerations

We determine first the optimum value of the anode wire resistance for simultaneous position and drift time measurements. In the case of the charge division alone the wire resistance R_D is determined by the readout linearity requirement and by the noise requirement, which pose opposite requirements on R_D. The equivalent noise charge is given by,[4,5]

$$\overline{ENC}_p^2 = 2kT \frac{1}{R_D} a_{F2} \tau_F \qquad (1)$$

where:

$R_D = R\ell$ = anode wire resistance
R = " " " per unit length
ℓ = " " length
a_{F2} = filter form factor
τ_F = time width of the filter weighting function

Clearly, R_D should be as high as possible for minimum noise from the resistive electrode. As shown previously,[4,5] a linear relation between the charge ratio $Q_A/(Q_A + Q_B)$ and the position is achieved for $\tau_F \geq R_D C_D$, where $C_D = C\ell$ is the anode wire capacitance. τ_F is usually determined by the charge collection time.

If timing is also of interest, then we have to determine the conditions for the shortest time for the distribution of the signal charge between the two ends of the anode wire. An anode wire with its surrounding electrodes (cathode wires, and/or field shaping wires in the drift chamber) represents a transmission line with distributed parameters R, L, C as illustrated in Fig. 2(a). (The conductance to ground is in this case clearly negligible). Two propagation mechanisms are possible depending on the relation of the line parameters. For small values of total line resistance ($R\ell$) the dominant mechanism is electromagnetic wave propagation, and for large values of $R\ell$ the dominant mechanism is diffusion. The latter case is usually assumed in charge division.

*Research was supported by the U. S. Department of Energy: Contract No. EY:76-C-02-0016.

A detailed analysis performed by the authors[6] shows that the shortest charge distribution time is achieved for,

$$R_D = R\ell = 2\pi \left(\frac{L}{C}\right)^{1/2} \quad . \qquad (2)$$

(This condition for transmission lines, corresponds to the "critical damping" condition for the lumped L, C, R tank circuit.) Two important properties of charge division have been proved:

1) the charge injected into the transmission line divides between the two ends in the line as $\tau \to \infty$ according to the ratio of resistances and independently of the value $R\ell$ and of the propagation mechanism;

2) the charge divides according to the ratio of resistances independently of the the distribution of inductance and capacitance along the transmission line.

The timing is performed on the sum signal from the two ends. For aperiodic response ($R_D \geq 2\pi(\frac{L}{C})^{1/2}$), the dominant term in the solution for the sum signal is given by,[5,6]

$$\frac{Q_A + Q_B}{Q_S} \approx 1 - \frac{4}{\pi} \exp(-\pi^2 t/\tau_D) \sin \pi \frac{x}{\ell} \qquad (3)$$

where $\tau_D = R_D C_D = RC\ell^2$.

The rise time of the sum signal varies from zero at the ends of the wire to a maximum value determined by the time constant,

$$\tau_r = \tau_D/\pi^2 \quad . \qquad (4)$$

The characteristic impedance $(L/C)^{1/2}$ of the anode wire in typical drift chamber configurations is of the order of 350 ohms, and the capacitance $C \approx 10$ pF/m. Nonmagnetic stainless steel wire* of 25 μm diameter has typically a resistance of 20 to 30 ohms/cm. An anode wire of the length of 1 meter satisfies Eq. (2). If the resistance is significantly lower than $2\pi(L/C)^{1/2} = 2200$ ohms, reflections will occur and the noise will be increased. If the resistance is higher, the rise time will be increased. The time constant τ_r in this case is 2.23 nsec. Since this response is faster than the signal resulting from the motion of positive ions, somewhat higher values of τ_r are acceptable with the benefit of lower noise. With a time constant τ_r of about 5 nsec, a timing uncertainty of 2 nsec or less can be achieved. This corresponds to a position error of $\sigma = 0.1$ mm (for an electron drift velocity of 5 cm/μsec). It is assumed here that the timing is performed on the leading edge of the signal, that is, ideally, on the "first electron". According to Eq. (3) the response of the diffusive line is position dependent. The contribution of the diffusion to the rise time varies from zero at the ends of the wire ($x = 0$) to $2.2\ \tau_r$ in the middle of the wire ($x = 1/2\ \ell$). The timing shift due to this is less than τ_r, and it requires a systematic correction, equivalent to that for the propagation time along the anode wire in drift chambers without charge division ($R_D \to 0$).

The width of one lobe of the filter bipolar trapezoidal weighting function should be larger than the maximum difference in the electron drift time in order to obtain a larger signal and a better measure of the energy loss ΔE. This is typically from 100 to 200 nsec.

With presently available wire alloys and a wire diameter of 25 μm an anode wire 1 meter long has an R_D = 2-3 kohms, $C \approx 10$ pF and τ_D = 20-30 nsec. A wire resistance of 5 - 10 kohm would be desirable in order to reduce the wire noise. For an anode wire 2 meters long (R_D = 4-6 kohm, $C \approx 20$ pF, τ_D = 80-120 nsec) all the parameters are better optimized. A larger wire diameter may be desirable in some cases because of higher mechanical strength. R_D should always be larger that 2 kohm in order to keep the noise sufficiently low. These considerations point to the need for higher resistivity wire alloys.

Charge division requires a low impedance connection between the two preamplifiers, and there is also an upper limit to the impedance connected between the electrode (or electrodes) surrounding the anode and ground. For timing, the integrity of the transmission line and its connections to the preamplifiers should be preserved. A well defined signal return path between the preamplifiers which includes the electrodes surrounding the anode is also essential to minimize the pickup of signals generated externally.

Finially, bypassing of the electrodes surrounding the anode is necessary to avoid the crosstalk among adjacent cells of a large drift chamber system. An electrode-preamplifier interconnection arrangement is shown in Fig. 2(b). The signal return is split into two parts, a dc and low frequency path, and a high frequency path through the bypass capacitor and the surrounding electrodes. An auxilliary wire at the anode potential (i.e., at ground potential) is required. Such a wire, with a low resistance ($r \ll R_D$), can be common for a number of the drift chamber cells and preamplifier pairs (two to twenty). Each surrounding electrode (field shaping wires or strips), which sees a portion of the induced charge from the anode, should be bypassed. For practical reasons (high voltage, stored energy, space) low values of bypass capacitors are preferable. Common capacitors can be used for electrodes at the same potential in different drift chamber cells. The minimum value of the total bypass capacitance C_b for one cell is determined by the signal charge feedback, as follows. The positive ion cloud drifting away from the anode produces a signal charge $-Q_S$ at the anode in the pulse shaping time τ_F. It also produces an equal amount of induced charge of opposite polarity on the surrounding electrode. The potential of the surrounding electrode is increased by Q_S/C_b. This in turn injects a charge into the anode proportional to the interelectrode capacitance C_D, that is, $Q_S \frac{C_D}{C_b}$. The injected charge is distributed uniformly along the wire with a centroid in the middle. The result of the charge division is then,

$$\frac{Q_A}{Q_A + Q_B} = \frac{Q_S \frac{x}{\ell} - \frac{1}{2}\frac{C_D}{C_b} Q_S}{Q_S - \frac{C_D}{C_b} Q_S} \approx \frac{x}{\ell}\left(1 + \frac{C_D}{C_b}\right) - \frac{1}{2}\frac{C_D}{C_b} \quad . \qquad (5)$$

This represents a downward shift in the origin of the straight line - the charge ratio versus the position - by $0.5\ C_D/C_b$, and an increase in its slope by $(1 + \frac{C_D}{C_b})$, (the line is rotated around its midpoint $x = \frac{1}{2}\ \ell$). This effect is stable (if C_b is stable) and it only requires a correction of the position data. $Q_S \frac{C_D}{C_b}$ also represents the total maximum amount of

*For example, Stablohm 800, California Fine Wire Co.

crosstalk from one cell to all adjacent cells, C_D/C_b of one percent with C_D = 10 pF in this case requires C_b = 1000 pF. C_b is split in half between the two ends of the chamber, and further subdivided among the surrounding electrodes according to the fraction of the anode image charge they "see".

Preamplifier

The charge divides in the anode wire according to the ratio of resistances and independently of the resistance value. The preamplifiers for charge division must have an input impedance which is low compared to the anode wire resistance in order to maximize the position sensitivity and to preserve the insensitivity of the position readout calibration against small variations in the anode wire resistance and differences in resistance from wire to wire. A low input impedance can be achieved by either a common base amplifier or by a feedback amplifier. Lower noise can be achieved by a feedback amplifier with a field-effect transistor at the input. However, the reproducibility of input impedance is easier to achieve with a common base amplifier. The common base input stage may be followed by a feedback charge amplifier as in some previous applications of charge division.[7,8] Alternatively, a common base input stage can be a part of a current-to-voltage amplifier. We have chosen the latter approach, since the faster (current) signal can be used directly for timing, and since the resulting circuit is somewhat simpler. (A current-to-voltage amplifier at the input requires an additional integration in the shaping amplifier.)

The basic circuit is shown in Fig. 3(a). The transfer impedance of the amplifier is determined by R_L and the dominant pole capacitance C_o. If $R_L C_o \ll \tau_F$, R_L is the only element determining the gain for charge division. C_o determines the "rate of rise" which is important for timing.

The optimum emitter current is determined by noise considerations. An analysis of the noise of a common base stage was presented in Reference 5. The optimum emitter current (and the emitter dynamic resistance) is a function of detector parameters R_D, C_D, transistor current gain h_{fe}, stray capacitance at the input, and of the filter weighting function. We take as an example here an anode wire with R_D = 2.2 kΩ, C_D = 25 pF, τ_D = 44 nsec, amplifier and connection stray capacitance C_A = 15 pF, h_{fe} = 100 and bipolar trapezoidal filter form factors[4,5] a_{F1} = 80 and a_{F2} = 1.46. Such a filter can be well approximated with double clipping and an RC integration. We assume here τ_F = 0.5 μsec and an integration time constant of 0.1 μsec. We use Eq. (18) from Ref. 5 to calculate the optimum emitter resistance,

$$\left(\frac{r_E}{R_D}\right)_{opt} = \frac{1}{h_{fe}^{\frac{1}{2}}} \left(1 + \frac{a_{F1}}{a_{F2}} \frac{\tau_C^2}{\tau_F^2}\right)^{-\frac{1}{2}} , \qquad (6)$$

where $\tau_C = R_D(C_D + C_A)$.

This gives $r_E \approx 134$ ohms, and with τ_F = 0.25 μsec we obtain r_E = 79 ohms. We use in the circuit in Fig. 3(b) r_E = 75 Ω which represents a fraction $\frac{r_E}{R_D + 2r_E}$ = 3.2 percent, of the total effective resistance of the charge division circuit. Obviously, if any of the values assumed in this example are significantly changed a new value of the optimum emitter resistance should be calculated. With r_E = 75 ohms, $I_E = kT/q_e r_E$ = 340 μA. In a simplified noise calculation, the shot noise in the base current I_{b1} and I_{b2}, and the thermal noise from the resistors R_{E1} and R_L should be added to the noise from the resistive electrode R_D. (The collector current shot noise is negligible if the impedance connected to the emitter is much higher than the equivalent series noise resistance $kT/2q_eI_E$ at all frequencies in the passband of the filter.) The total noise from these additional sources is equivalent to the thermal noise of a resistance of 4.3 kohms. The noise of the position readout is then determined by a parallel combination of this resistance and R_D. We calculate the equivalent noise charge, Eq. (1),

$$ENC_p \approx 1.3 \times 10^4 \text{ rms electrons} \quad . \qquad (7)$$

This noise is higher by 23% than the resistive wire noise, due to the amplifier noise.

The main concern in the implementation of this preamplifier is to minimize the dominant pole capacitance C_o. This can be achieved by using transistors with a low collector-to-base capacitance C_{ob} and a high unity gain frequency f_T. The lowest values of C_o can be realized in hybrid and integrated circuit techniques. If these techniques are not available, an alternative is to use a monolithic transistor array with external resistors, as shown in Fig. 3(b). The collector-to-base capacitance of the transistors in the array used here is, $C_{cb} \leq 0.2$ pF. The much larger collector-to-substrate capacitance ($C_{cs} \approx 1.6$ pF) of the first transistor is virtually cancelled by "bootstrapping" the substrate of the array to the output emitter. A very low dominant pole capacitance is thus achieved, $C_o \approx 0.6$ pF.

With fast high gain amplifiers certain layout rules should be carefully observed. They are illustrated in Fig. 4 for this case. The stray feedback capacitance should be much smaller than C_o, since it represents positive feedback and would cause instability if $C_{sf} \geq C_o$. C_{sc} causes crosstalk, and it should also be smaller than C_o. All other stray capacitances from inputs and outputs to ground, from input-to-input and from output-to-output can be larger, since these are low impedance points. These rules allow high density mounting of amplifiers in a large system, where shielding of all inputs from all outputs is provided.

Results

The properties of the readout were studied on an experimental cylindrical detector as a model of a single cell of a drift chamber with the following parameters: length ℓ = 217 cm; anode diameter 25 μm; cathode diameter 1.5 cm; anode wire resistance R_D = 2200 ohms; anode wire capacitance $C_D \approx 25$ pF; cathode bypass capacitance C_b = 940 pF; gas: argon 90% + methane 10%. A long anode wire was chosen in order to make more accurate the relative position resolution and the nonlinearity measurements. A lower resistivity wire was used to obtain total resistance corresponding to more typical cases of anode wire lengths of about 1 meter with higher resistivity wires, and to study the case of critical damping, Eq. (2). A system with an analog divider[9] was used for these measurements.

The position resolution as a function of the signal charge, and the detector voltage is shown in Fig. 5. The measured position resolution agrees well with the noise calculated in the preceding section. FWHM of 1% is achieved with a signal $Q_S \approx 0.5$ picocoulombs. According to Eq. (1) the noise is proportional to $\tau_F^{\frac{1}{2}}$. The observed signal charge is approximately a logarithmic function[4] of τ_F. The resulting measured values of the position resolution as a function of τ_F, with the same gas gain, are:

τ_F[μsec]	FWHM[%]	σ[%]
1	1.3	0.55
0.5	1.0	0.43
0.25	0.78	0.33

The shortest τ_F to be used with charged particles is determined by the difference in electron drift time between the first and the last primary electrons arriving at the anode, if the energy loss ΔE is also measured. If ΔE information is not required, shorter values of τ_F can be used (≈ 0.1 μsec) for operation at higher event rates.

The same position resolution was measured with an x-ray source and a pulse generator. The resolution was constant within ± 5% along the wire length.

Figure 6 shows the position calibration. The readout is linear, and the calibration straight line corresponds accurately to the theoretical one, which takes into account the amplifier input resistance and the finite cathode bypass capacitance. Note that the pulses injected at the ends of the wire through R_{E1} (or through a small capacitance) are not subject to the finite bypass effect.

Figures 7 and 8 show signal waveforms at the output of the preamplifier, taken with a storage oscilloscope so that single traces could be recorded. Figures 7(a) and 8 are 5.9 keV x-rays at $x = \ell/2$. Figures 7(b) and (c) were taken with minimum ionizing particles traversing the detector at the anode wire and they show the fluctuations in the energy loss along the particle track. Figure 9 shows the output of the shaping amplifier for x-rays (a) and for minimum ionizing particles (b).

The timing resolution is determined by the noise and by the signal slope at the output of the timing channel. The preamplifiers are followed by an RC differentiation with a time constant of 20 nsec, and an integration of 5 nsec, which maximizes the signal slope-to-noise ratio for this detector (different values of time constants might be required for different gases and electrode dimensions). We have measured an equivalent noise charge in the timing channel, $ENC_t \approx 1.9 \times 10^4$ rms electrons, and a signal slope at the beginning of the leading edge of $\frac{dS(t)}{dt} \approx 0.04\ Q_S$/nsec, where Q_S is referred to as the charge measured with $\tau_F = 0.5$ μsec. The slope was measured with 5.9 keV x-rays which produce localized primary ionization. The timing error is then,

$$\sigma_t = ENC_t \frac{1}{\frac{dS(t)}{dt}} = \frac{4.7 \times 10^5}{Q_S[e]}\ [\text{nsec}] \quad . \qquad (8)$$

For $\sigma_t = 2$ nsec, which corresponds to an uncertainty of about 0.1 mm in the position coordinate determined by electron drift (in argon), the signal charge required is $Q_S \approx 2.4 \times 10^3$ electrons. This is quite a small amount for x-rays. In the case of minimum ionizing particles, this amount of charge should be produced by the cluster of primary electrons which arrives first at the anode (corresponding to the first component of the signals shown in Figs. 7(b) and (c)). In typical drift chambers, this corresponds to a most probable total signal charge of 10^6 to 2×10^6 e, which allows their operation in the linear range.

Acknowledgements

Discussions with W. J. Willis on the use of drift chambers in experiments at intersecting storage rings, with J. L. Alberi on charge division readouts, and with J. Fischer and A. H. Walenta on the drift chambers are gratefully acknowledged. L. C. Rogers collaborated on the preamplifier design and testing.

References

1. R. Bosshard, R. L. Chase, J. Fischer, S. Iwata, and V. Radeka, IEEE Trans. Nucl. Sci., NS-22 (1975) 2053.
2. H. Okuno, R. L. Chase, J. Fischer, and A. H. Walenta, IEEE Trans. Nucl. Sci., NS-24, (Feb. 1977) 213-217.
3. M. Atac, R. Bosshard, S. Erhan, and P. Schlein, IEEE Trans. Nucl. Sci., NS-24, (Feb. 1977) 195-199.
4. V. Radeka, IEEE Trans. Nucl. Sci., NS-21 (Feb. 1974) 51.
5. J. L. Alberi and V. Radeka, IEEE Trans, Nucl. Sci., NS-23, (Feb. 1976) 251-258.
6. V. Radeka, P. Rehak, to be published.
7. P. Schübelin, J. Fuhrmann, S. Iwata, V. Radeka, W. N. Schreiner, F. Turkot, A. Weitsch, and R. W. Sancton, Nucl. Instr. & Meth., 131 (1975) 39-46.
8. J. Fischer, J. Fuhrmann, S. Iwata, R. Palmer and V. Radeka, Nucl. Instr. & Meth., 136 (1976) 19-27.
9. J. Alberi, J. Fischer, V. Radeka, L. C. Rogers and B. Schoenborn, Nucl. Instr. & Meth., 127 (1975) 507.

Figure Captions

Fig. 1: Dual coordinate readout in drift chambers by charge division.
y - high precision coordinate,
$\sigma \approx 0.1$ mm by electron drift.

x - lower precision coordinate,
$\sigma \approx 0.5$ percent of the anode wire length.

The sum signal $Q_A + Q_B$ is a measure of the energy loss ΔE in the detector.

Fig. 2: (a) division of charge in transmission lines;
(b) signal return in proportional (drift) chamber and preamplifier configurations.

Fig. 3: Fast "current" preamplifier for charge division:

(a) basic circuit;
(b) preamplifier circuit using a monolithic transistor array (RCA CA3127E).

Fig. 4: Crosstalk and parasitic feedback in preamplifiers. $C_{S\ in}$ and $C_{S\ out}$ are allowed, while C_{sf} and C_{sc} should be much smaller than the dominant pole capacitance C_o (Fig. 3).

Fig. 5: Position resolution as a function of signal charge measured with 5.9 keV x-rays. Bipolar double delay line shaping with τ_F = 0.5 μsec was used. For τ_F = 1 μsec FWHM should be multiplied by 1.3 and for τ_F = 0.25 μsec by 0.78.

Fig. 6: Charge ratio as a function of the source position.

Fig. 7: Signal waveforms at the output of the preamplifier.

(a) for 5.9 keV x-rays;
(b) and (c) two samples of waveforms for minimum ionizing particles.

Fig. 8: Same as Fig. 7(a) with expanded time scale.

Fig. 9: Signal waveforms at the output of the shaping amplifier.

(a) for 5.9 keV x-rays;
(b) for minimum ionizing particles.

τ_F = 0.5 μsec, τ_i = 0.1 μsec.

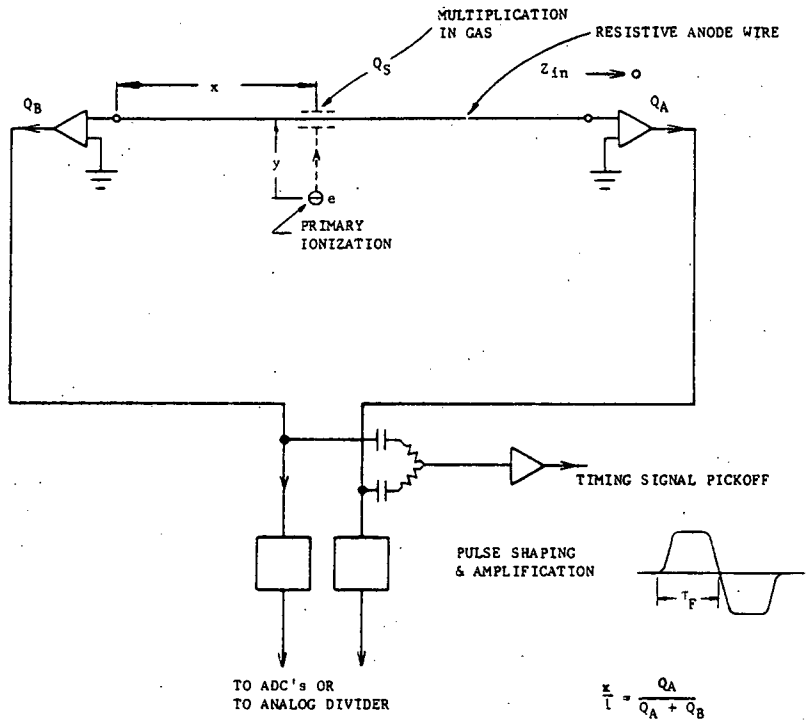

FIGURE 1

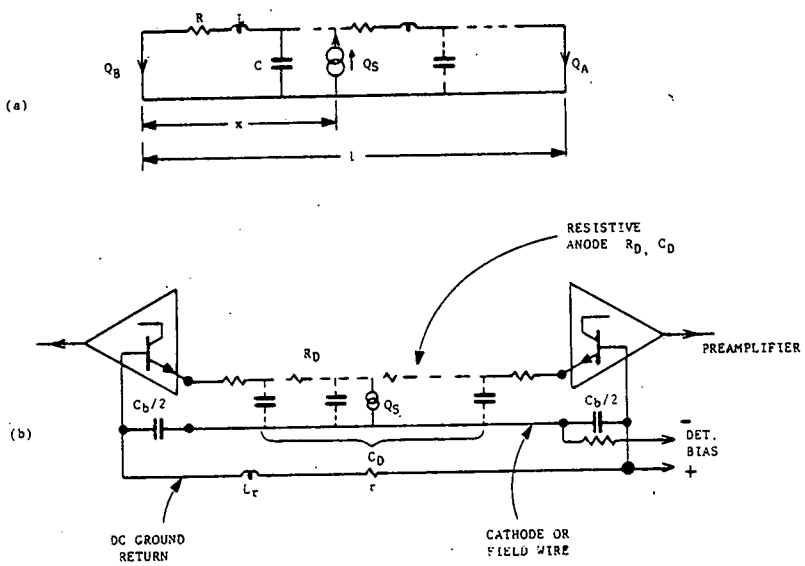

FIGURE 2

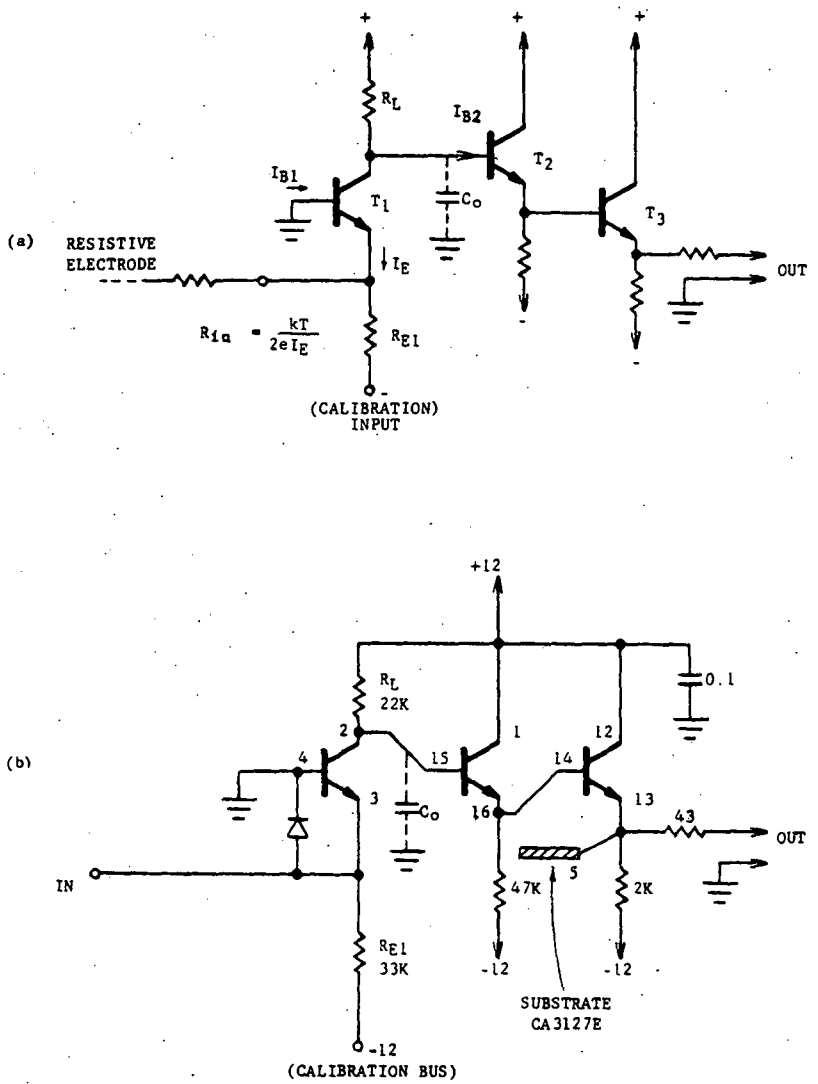
(a)
RESISTIVE ELECTRODE
R_L
I_{B2}
T_2
I_{B1}
T_1
C_o
T_3
I_E
OUT
$R_{in} = \frac{kT}{2eI_E}$
R_{E1}
(CALIBRATION) INPUT
(b)
+12
R_L 22K
0.1
2
1
12
4
15
14
3
C_o
16
13
43
OUT
IN
47K
5
2K
R_{E1} 33K
-12
-12
SUBSTRATE CA3127E
-12
(CALIBRATION BUS)

FIGURE 3

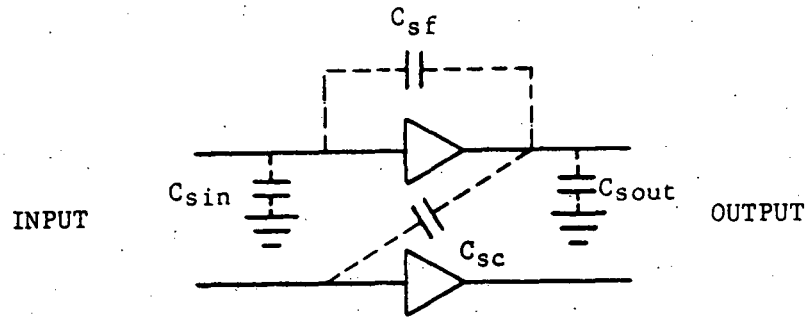

FIGURE 4

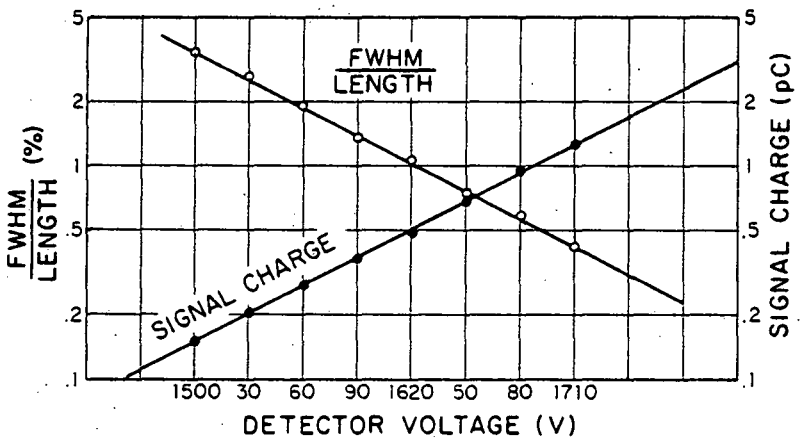

FIGURE 5

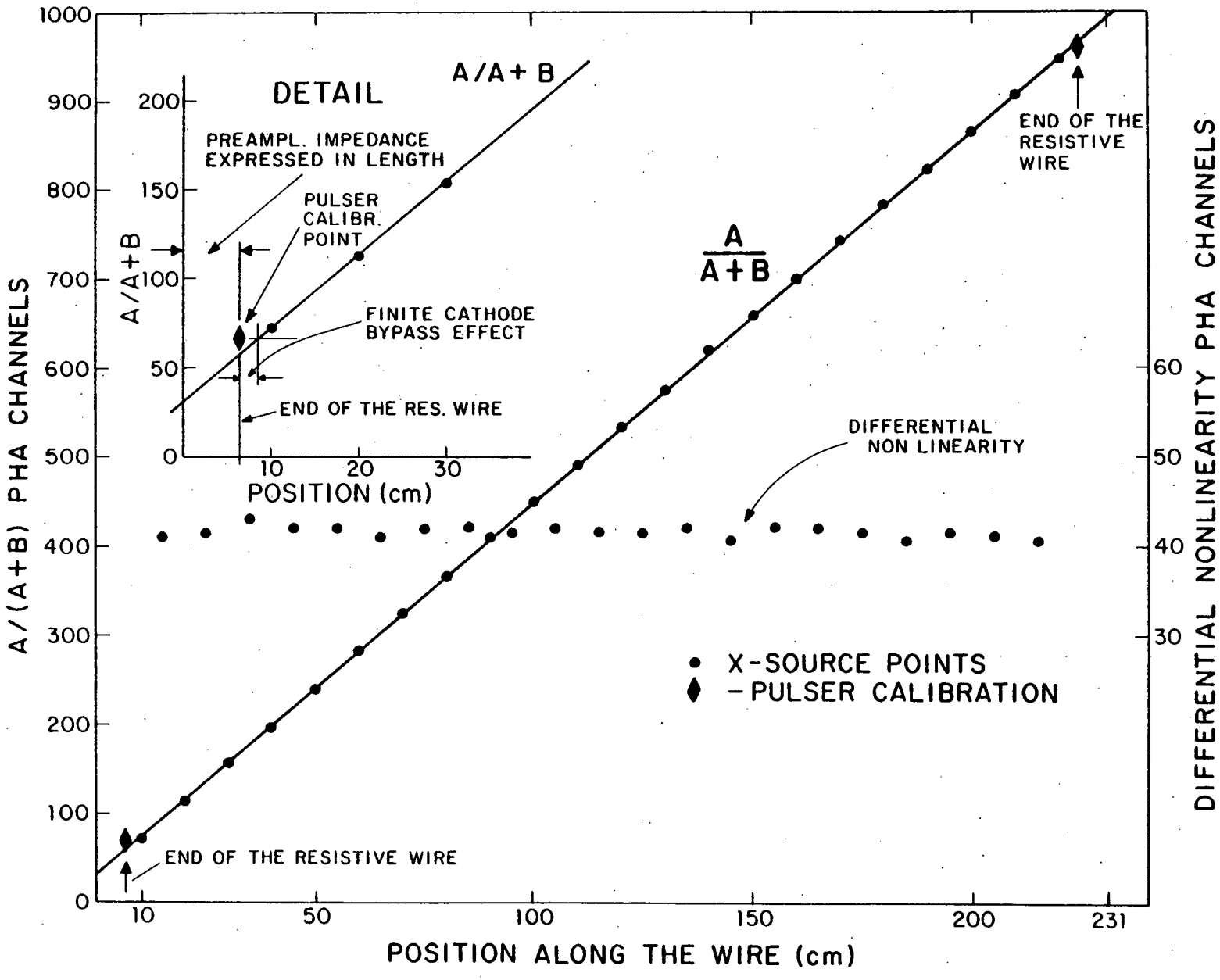
DETAIL
A/A+ B
PREAMPL. IMPEDANCE EXPRESSED IN LENGTH
PULSER CALIBR. POINT
FINITE CATHODE BYPASS EFFECT
END OF THE RES. WIRE
A/A+B
POSITION (cm)
A/(A+B) PHA CHANNELS
A / A+B
END OF THE RESISTIVE WIRE
DIFFERENTIAL NON LINEARITY
X-SOURCE POINTS
-PULSER CALIBRATION
END OF THE RESISTIVE WIRE
POSITION ALONG THE WIRE (cm)
DIFFERENTIAL NONLINEARITY PHA CHANNELS

FIGURE 6

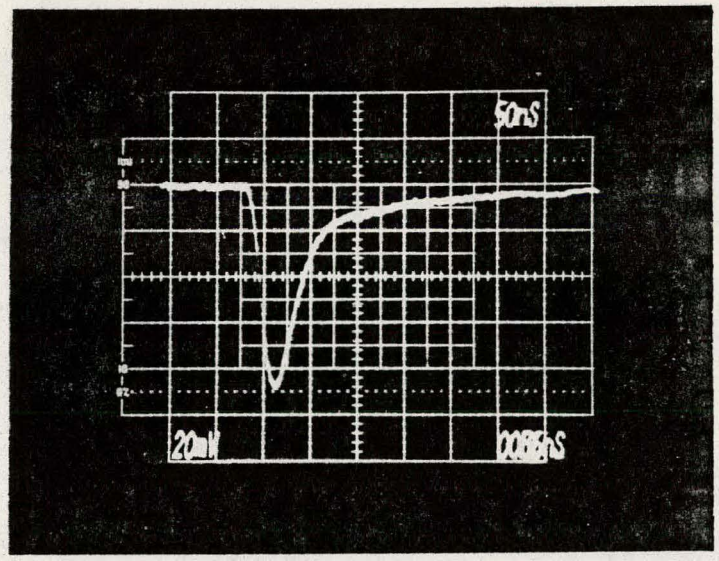

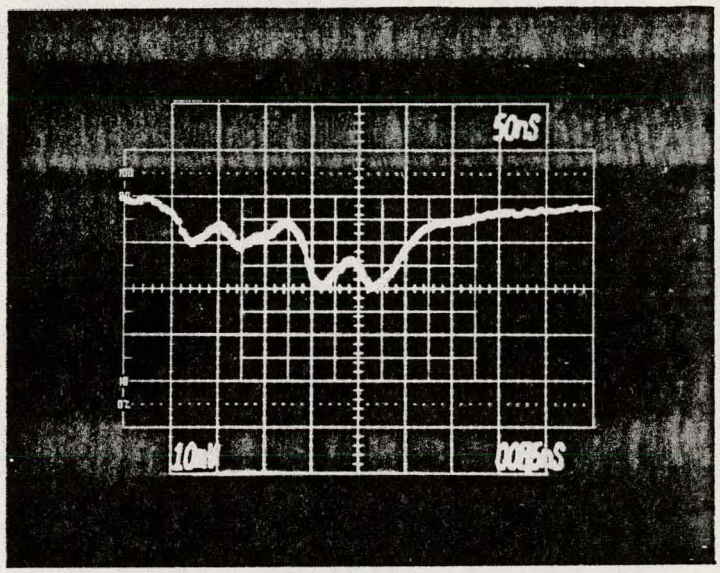

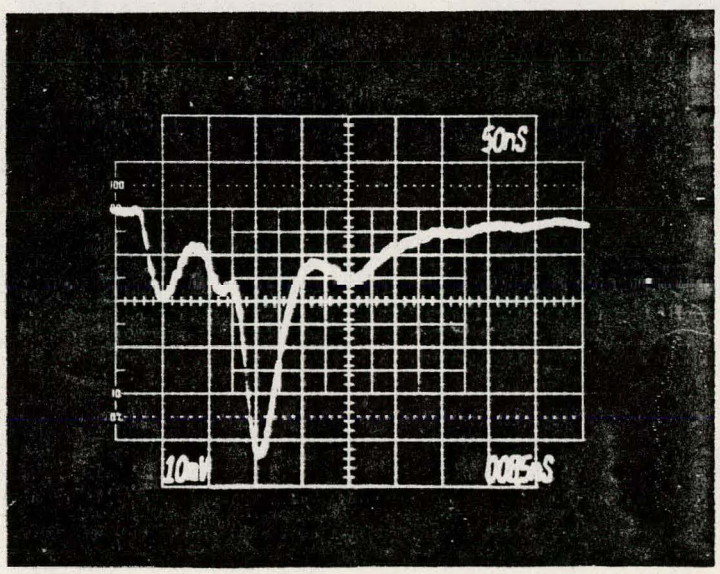

FIGURE 7

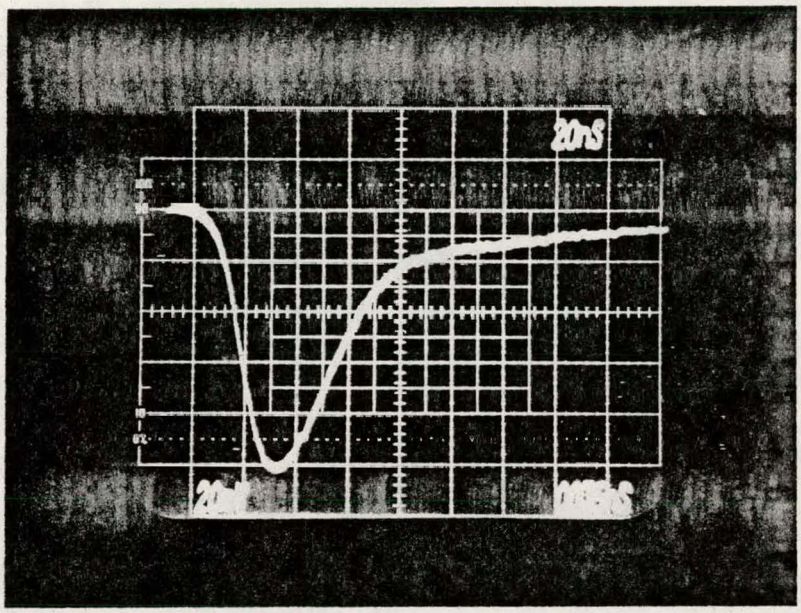

FIGURE 8

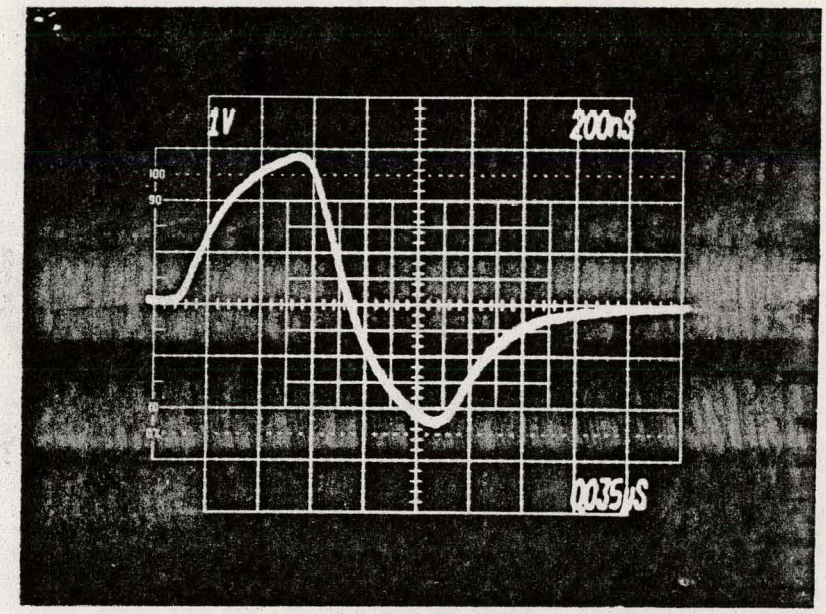

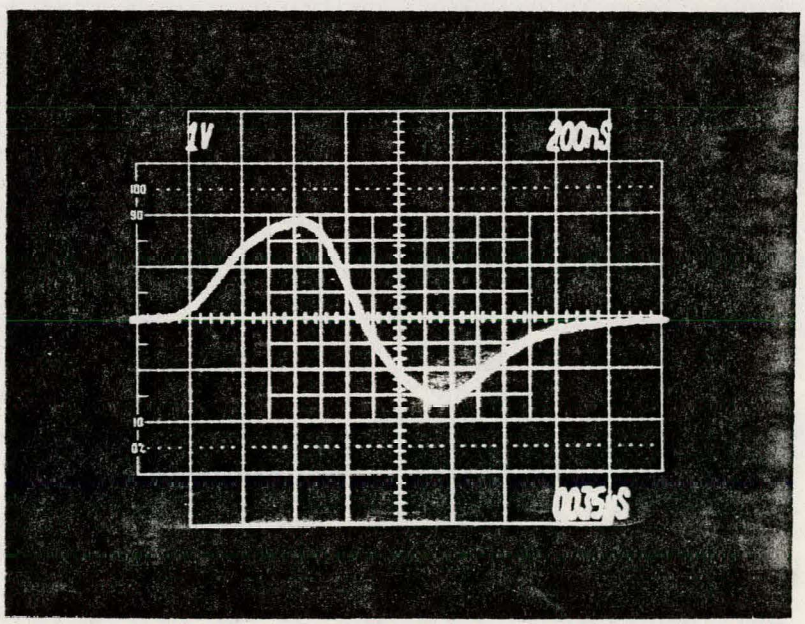

FIGURE 9